A Cohesive Model for Fatigue Crack

Anna Pandolfi[1] and Michael Ortiz[2]

[1] Dipartimento di Ingegneria Strutturale – Politecnico, Milano (Italy)
[2] Graduate Aeronautical Laboratories – Caltech, Pasadena (USA)

ABSTRACT. *We describe fatigue processes within the framework of cohesive theories of fracture. Crack formation is due to the gradual separation of material surfaces resisted by cohesive tractions. The relationship between traction and opening displacement is governed by an irreversible law with unloading-reloading hysteresis. We assume that the unloading-reloading response of the cohesive model degrades with the number of cycles and assume the reloading stiffness as damage variable. The fatigue behavior is embedded into surface-like finite elements, compatible with a standard discretization of solid volumes. The potential fatigue cracks are identified by inter-element surfaces, initially coherent. When a fatigue initiation criterion is satisfied, a self-adaptive remeshing procedure inserts a cohesive element.*

INTRODUCTION

The centerpiece of the present approach is the description of the fracture processes by means of an irreversible cohesive law with unloading-reloading hysteresis. The separation of the crack surfaces is resisted by cohesive tractions. Monotonic loading of the crack defines a cohesive envelope. In this paper, cohesive envelope is described through the universal binding law by Smith-Ferrante [1] slanted so that the initial slope is infinite. The behavior of the material under cyclic loading requires a degradation of the unloading-reloading response with the number of cycles. Additionally, the model accounts for mixed loading conditions by recourse to effective scalar variables. These variables are built using a constitutive parameter, which assigns a different weight to normal and sliding components of the corresponding vectors.

MONOTONIC LOADING

We start by considering monotonic loading processes resulting in pure mode I opening of the crack. As the incipient fracture surface opens under the action of the loads, the opening is resisted by a number of material-dependent mechanisms. We assume that the resulting cohesive traction T follows the universal binding law proposed in [1], slanted so that the initial slope is infinite. The cohesive law reaches a critical stress T_c upon the attainment of a critical opening displacement δ_c, Fig. 1a. The relation between T and δ under monotonic opening is referred as the monotonic cohesive envelope.

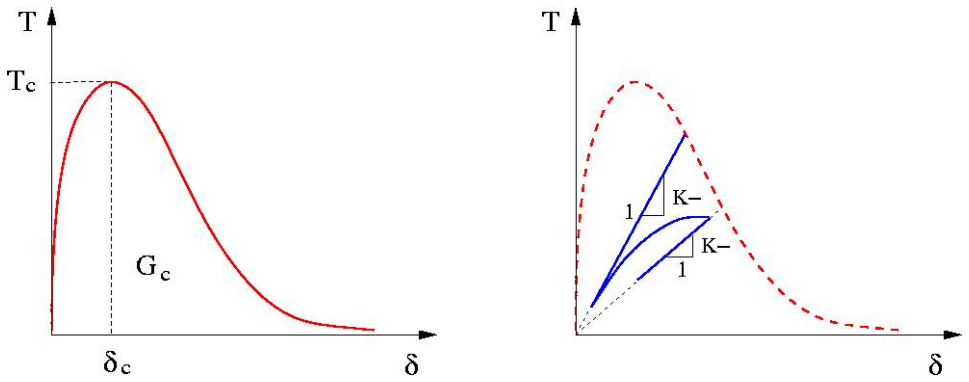

Figure 1. a) Cohesive law with Modified Smith-Ferrante envelope; b) Cyclic cohesive law with unloading-reloading hysteresis.

The critical stress T_c may be identified with the macroscopic cohesive strength or the spall strength of the material. The area under the monotonic cohesive envelope equals the critical energy release rate G_c of the material.

CYCLIC BEHAVIOR

The cohesive behavior of the material under cyclic loading is of primary concern [4]. Let us consider a cohesive surface cycled at low amplitude after unloading from the monotonic cohesive envelope, and assume that the amplitude of the loading cycle is less than the height of the monotonic envelope at the unloading point, Fig. 1b.

Experimental observations show that the unloading-reloading response degrades with the number of cycles (for example, repeated rubbing of asperities may result in wear or polishing of the contact surfaces, provoking steady weakening of the cohesive response). A simple phenomenological model which embodies these assumptions is obtained by assuming different incremental stiffnesses depending on whether the cohesive surface opens or closes, i.e.,

$$\dot{T} = \begin{cases} K^{-}\dot{\delta}, & \text{if } \dot{\delta} < 0 \\ K^{+}\dot{\delta}, & \text{if } \dot{\delta} > 0 \end{cases} \tag{1}$$

where K^+ and K^- are the loading and unloading incremental stiffnesses respectively. We take the stiffnesses $K^{\pm}$ to be internal variables in the spirit of damage theories, and their evolution to be governed by suitable kinetic equations. Assume for simplicity that unloading always takes place towards the origin of the T-δ axes, i.e.,

$$K^{-} = \frac{T_{max}}{\delta_{max}} \tag{2}$$

where T_{max} and δ_{max} are the traction and opening displacement at the point of load reversal, respectively. K^- remains constant for as long as crack closure continues. By contrast, the reloading stiffness K^+ is assumed to evolve in accordance with the following kinetic relation:

$$\dot{K}^+ = \begin{cases} -K^+ \dot{\delta} / \delta_f, & \text{if } \dot{\delta} < 0 \\ \left(K^+ - K^-\right)\dot{\delta} / \delta_f, & \text{if } \dot{\delta} > 0 \end{cases} \tag{3}$$

The parameter δ_f is a characteristic opening displacement. It can be observed that, upon unloading, K^+ tends to the unloading slope K^-, whereas, upon reloading, K^+ degrades steadily, Fig. 1b.

Finally, we assume that the cohesive traction cannot exceed the monotonic cohesive envelope. Consequently, when the stress-strain curve intersects the envelope during reloading, it is subsequently bound to remain on the envelope for as long as the loading process ensues. Fig. 2 shows the effect of changing the parameter δ_f under cyclic loading.

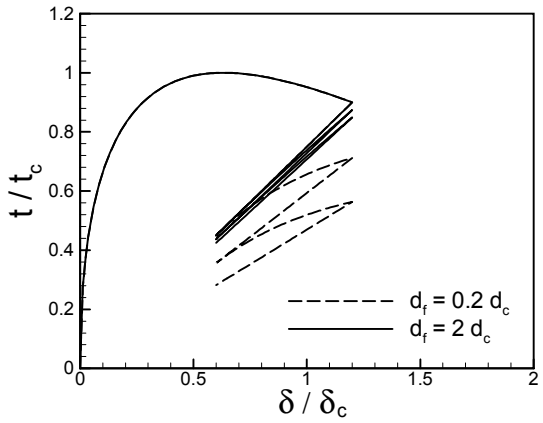

Figure 2. Effect of the parameter δ_f of the response of the model under cycling.

The details of the kinetic equations for the unloading and reloading stiffnesses just described are largely arbitrary, and the resulting model is very much phenomenological in nature. However, some aspects of the model may be regarded as essential and are amenable to experimental validation. Assuming a constant amplitude displacement cycling, it can be observed that –to first order approximation— the model predicts an exponential decay for the maximum traction. This is an essential feature of the model, which can be tested experimentally.

EXTENSION TO MIXED MODE

To account for mixed loading and combined opening and sliding, we follow [5,6] and introduce the effective opening displacement (see Fig. 3)

$$\delta = \sqrt{\beta^2 \delta_S^2 + \delta_n^2}, \quad \delta_n = \boldsymbol{\delta} \cdot \mathbf{n}, \quad \boldsymbol{\delta}_S = \boldsymbol{\delta} - \delta_n \mathbf{n} \tag{4}$$

where the parameter β assigns different weights to the sliding δ_S and normal δ_n opening displacements. A simple model of cohesion is obtained by assuming that the free energy potential ϕ depends on $\boldsymbol{\delta}$ only through the effective opening displacement δ, i. e., $\phi = \phi(\delta, \mathbf{q})$. The cohesive law reduces to:

$$\mathbf{t} = \frac{\partial \phi}{\partial \boldsymbol{\delta}} = \frac{t}{\delta}\left(\beta^2 \boldsymbol{\delta}_S + \delta_n \mathbf{n}\right), \quad t = \frac{\partial \phi}{\partial \delta}(\delta, \mathbf{q}) = \sqrt{\beta^{-2}\left|\mathbf{t}_S\right|^2 + t_n^2}, \quad t_n = \mathbf{t} \cdot \mathbf{n}, \quad \mathbf{t}_S = \mathbf{t} - t_n \mathbf{n} \tag{5}$$

where we introduce the effective traction t.

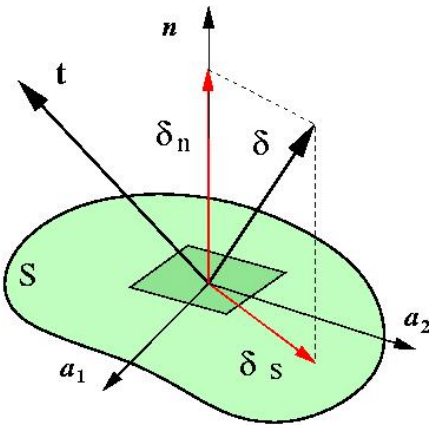

Figure 3. Decomposition of the opening displacement into the normal and the sliding component.

Relation (5b) shows that β defines the ratio between the shear and the normal critical tractions. In brittle materials, this ratio may be estimated by imposing lateral confinement on specimens subjected to high-strain-rate axial compression [3, 4].

Upon closure, the cohesive surfaces are subject to the contact unilateral constraint, including friction. We regard contact and friction as independent phenomena to be modeled outside the cohesive law. Friction may significantly increase the sliding resistance in closed cohesive surfaces. In particular, the presence of friction may result in a steady —or even increasing— frictional resistance while the normal cohesive strength simultaneously weakens.

COHESIVE-FATIGUE FINITE ELEMENT

The cohesive-fatigue behavior has been implemented in finite elements, in a finite kinematics framework. The class of elements considered consists of two surface elements which coincide in space in the reference configuration of the solid, Fig. 4a. One of the surface elements is designated as S^- and the remaining one as S^+. Each of the surface elements has n nodes. The total number of nodes of the cohesive element is, therefore, $2n$. The particular triangular geometry depicted in Fig. 4a is compatible with three-dimensional tetrahedral elements, Fig. 4b.

The behavior of a cohesive surface may be expected to differ markedly depending on whether the surface undergoes sliding or normal separation. This requires the continuous tracking of the normal and tangential directions to the surface. In particular, since S^- and S^+ may diverge by a finite distance, the definition of a unique normal direction $\mathbf{n}$ is to some extent a matter of convention.

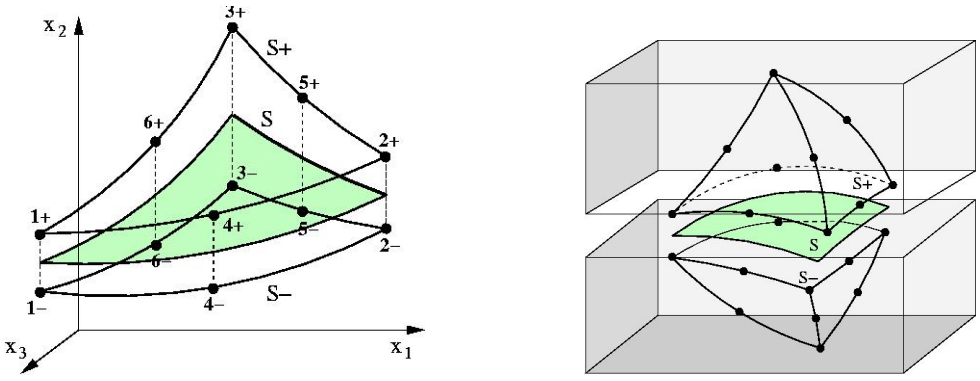

Figure 4. a) Geometry of cohesive element; b) Assembly of 12-node triangular cohesive element and two 10-node tetrahedral elements.

We assume that all geometrical operations such as the computation of the normal are carried out on the *middle surface* S of the element, Fig. 4a, defined parametrically as

$$\mathbf{x}(\mathbf{s}) = \sum_{a=1}^{n} \bar{\mathbf{x}}_a N_a(\mathbf{s}), \qquad \bar{\mathbf{x}}_a = \frac{1}{2}\left(\mathbf{x}_a^+ + \mathbf{x}_a^-\right) \tag{6}$$

where we denote by $N_a(s_1, s_2)$ the standard shape functions (a = 1,…, n) of each of the constituent surface elements and by $\mathbf{x}_a$ the coordinates of the nodes in the deformed configuration of the element. The coordinates s_1, s_2 are the natural coordinates of each of the surface elements in some convenient standard configuration. The unit normal can thus be easily computed through the tangent basis vectors [6].

The opening displacement vector in the deformed configuration (remains invariant upon superposed rigid translations of the element) is:

$$\boldsymbol{\delta}(\mathbf{s}) = \sum_{a=1}^{n} \| \mathbf{x}_a \| N_a(\mathbf{s}), \qquad \| \mathbf{x}_a \| = \mathbf{x}_a^+ - \mathbf{x}_a^- \tag{7}$$

For the cohesive model described by (5a), the cohesive tractions per unit undeformed area follow as

$$\mathbf{t} = \frac{t}{\delta}\left[\beta^2 \boldsymbol{\delta}_S + (1-\beta^2)(\boldsymbol{\delta}\cdot\mathbf{n})\mathbf{n} \right] = \mathbf{t}(\boldsymbol{\delta}, \mathbf{n}) \tag{8}$$

The dependence of **t** on the normal **n** in (8) needs to be carefully accounted for in a finite deformation setting as it leads to geometrical terms in the tangent stiffness matrix. The nodal forces now follow from the tractions as

$$f_{ia}^{\pm} = \mp \int_{S_0} t_i N_a dS_0 \tag{9}$$

The integral extends over the undeformed surface of the element in its reference configuration. The tangent stiffness matrix follows by consistent linearization of (9), with the result below:

$$K_{iakb}^{\pm\pm} = \mp \mp \int_{S_0} \frac{\partial t_i}{\partial \delta_k} N_a N_b dS_0 \mp \frac{1}{2} \int_{S_0} \frac{\partial t_i}{\partial n_p} \frac{\partial n_p}{\partial \bar{x}_{kb}} N_a dS_0 \tag{10}$$

The geometrical terms in (10) render the stiffness matrix unsymmetric [6].

INSERTION CRITERIA

In numerical simulations of crack nucleation and propagation, we make use of a self-adative procedure able to insert cohesive elements along inter-element surfaces originally coherent [8]. The insertion of a cohesive-fatigue element can be driven by several criteria, in the sense that different variables can be adopted as indicator for the creation of new inter-element cohesive surfaces. Examples of such variables can be an equivalent strain measure, the deformation energy density, or the effective traction acting on the interface.

In our previous numerical experiments, we found out that the effective traction is a reliable indicator [8]. The stress variables are computed at the integration points of the bulk elements. Using the shape functions, it is possible to extrapolate the stress values into the gauss points on the element interfaces. Once the stress tensor is known at these points, the traction **t** acting on the normal **n** to the element (that will become the cohesive surface) is computed as:

$$\mathbf{t} = \boldsymbol{\sigma} \cdot \mathbf{n} \tag{11}$$

and decomposed into the normal t_n and tangential t_S component. The opening criterion is satisfied, therefore the facet labelled for opening, if the effective traction t reaches a suitable threshold t_{max}:

$$t = \sqrt{t_n^2 + \beta^{-2} t_S^2} \geq t_{max} \tag{12}$$

t_{max} is an additional material property, related to the tensile strength of the material, and in the most cases can be assumed equal to a certain percentage of T_c.

REFERENCES

1. Rose, J.H., Ferrante, J., Smith, J.R. (1981) Universal binding energy curves for metals and bimetallic interfaces, Physical Review Letters, **47** (9), 675-678.
2. Planas, J., Elices, M. (1991) Nonlinear fracture of cohesive materials, *Internationla Journal of Fracture*, **3**, 139-157.
3. Chen, W.N., Ravichandran, G. (1994) Dynamic compressive behavior of ceramics under lateral confinement, *Journal de Physique IV*, **4**, 177-182.
4. Chen, W.N., Ravichandran, G. (1996) Static and dynamic compressive behavior of aluminum nitride under moderate confinement, *Journal of the American Ceramic Society*, **79**, 579-584.
5. Camacho, G.T., Ortiz, M. (1996) Computational modelling of impact damage in brittle materials, *International Journal of Solids and Structures*, **33** (20-22), 2899-2938.
6. Ortiz, M., Pandolfi, A. (1999) A class of cohesive elements for the simulation of three-dimensional crack propagation, *International Journal for Numerical Methods in Engineering*, **44**, 1267-1282.
7. Nguyen, O., Repetto, E., Ortiz, M., Radovitzky, R. (2001) A cohesive model of fatigue crack growth, *International Journal of Fracture*, **110**, 351-369.
8. Pandolfi, A., Ortiz, M. (2002) An efficient adaptive procedure for three-dimensional fragmentation simulations, *Engineering with Computers*, **18** (2), 148-159.